Measuring hydraulic fracture apertures: a comparison of methods

Chaojie Cheng[1,2], Sina Hale[3], Harald Milsch[1], Philipp Blum[3]

[1] GFZ German Research Centre for Geosciences, Section 4.8 Geoenergy, Telegrafenberg, 14473 Potsdam, Germany
[2] University of Potsdam, Institute for Geosciences, Karl-Liebknecht-Str. 24-25, 14476 Potsdam, Germany
5 [3] Karlsruhe Institute of Technology (KIT), Institute of Applied Geosciences (AGW), Adenauerring 20b, 76131 Karlsruhe, Germany

Correspondence to: Harald Milsch (milsch@gfz-potsdam.de)

Abstract. Hydraulic fracture apertures predominantly control fluid transport in fractured rock masses. Hence, the objective of the current study is to investigate and compare three different laboratory scale methods to determine hydraulic apertures in
10 fractured (Fontainebleau and Flechtinger) sandstone samples with negligible matrix permeability. Direct measurements were performed by using a flow-through apparatus and a transient-airflow permeameter. In addition, a microscope camera permitted to measure the mechanical fracture apertures from which the corresponding hydraulic apertures were indirectly derived by applying various empirical correlations. Single fractures in the sample cores were generated artificially either by axial splitting or by a saw cut resulting in hydraulic apertures that ranged between 8 μm and 66 μm. The transient-airflow permeameter
15 shows accurate values in comparison to the flow-through derived results, in particular when repeated measurements along the full fracture width are performed. In this case, the derived hydraulic fracture apertures are in an excellent quantitative agreement. When hydraulic apertures are calculated indirectly from optically determined mechanical apertures using empirical equations, aperture differences between samples are merely reproduced qualitatively. Variations in hydraulic apertures as observed between methods are almost certainly related to differences in sampled fracture volume. Overall, using direct flow-
20 through measurements as a reference, this study demonstrates the applicability of mobile methods to determine hydraulic fracture apertures at both the laboratory and outcrop scales.

1 Introduction

The aperture of fractures in rock, allowing for fluid flow, mainly controls the transport properties of fractured rock masses with low matrix permeability. This quantity is of significant importance for both natural fluid flow within the Earth's crust and
25 geotechnical applications such as oil and gas exploitation in petroleum reservoirs, hydrothermal fluid flow in geothermal systems, and the underground storage of nuclear waste. Thus, reliable and accurate methods for determining fracture aperture and therefore the permeability of fractured rocks are essential.

The hydraulic aperture representing the capability of fluid flow through a rock fracture is typically derived by using a parallel plate model (Snow, 1969; Neuzil and Tracy, 1981). For the laminar flow of an incompressible Newtonian fluid between two
30 smooth and parallel plates, the flow rate is proportional to the third power of hydraulic aperture, which is commonly referred

to as the "cubic law" (Witherspoon et al., 1980). In contrast, the mechanical aperture is defined as the arithmetic average distance between the adjacent fracture walls measured perpendicular to a reference plane (Hakami and Larsson, 1996; Renshaw et al., 2000). Previously, the relative roughness expressed by the ratio of the standard deviation of the measured mechanical aperture and the mean mechanical aperture was used to estimate hydraulic fracture aperture (Zimmerman et al., 1991;

35 Renshaw, 1995; Barton and de Quadros, 1997; Xiong et al., 2011; Kling et al., 2017). In addition, a correlation between hydraulic and mechanical aperture was established introducing the contact area ratio, defined as the ratio of the true contact area of fracture asperities and the apparent total fracture surface area of a single fracture (Walsh, 1981). As a result, the hydraulic aperture of a single fracture can be determined either directly by using the "cubic law" or indirectly based on the mechanical aperture.

40 Typically, the evaluation of the hydraulic aperture is often performed on fractured core samples using flow-through apparatuses at the laboratory scale. Moreover, outcrop studies are widely used to characterize fracture patterns involving, e.g., orientations, distribution, length, and networks within a certain reservoir unit to evaluate its hydraulic performance (Zeeb et al., 2013). Apertures (here the opening width of the fracture, i.e., the mechanical aperture) are rarely measured universally due to difficulties impeding accurate measurements (Watkins et al., 2015) such as surface weathering, limits of resolution, and

45 measurement efficiency. Lately, portable devices such as airflow permeameters, which are more efficient and less costly in comparison to flow-through tests, were developed to investigate both porous rocks and fractures on outcrop profiles (Brown and Smith, 2013). With such devices, large outcrop surfaces as well as anisotropy in a porous rock's transport properties were investigated previously (Huysmans et al., 2008; Rogiers et al., 2013, 2014). However, the reliability of this approach for natural rough fractures remains to be elucidated since the basic calibration of such measurements is only performed using parallel-

50 plate fractures.

Furthermore, the hydraulic aperture of a fractured rock can also be characterized indirectly by statistical measurements of mechanical aperture such as image analysis of fracture profiles performed by progressively grinding an epoxy resin-fixed sample in pre-defined intervals (Snow, 1970; Hakami and Larsson, 1996; Konzuk and Kueper, 2004), fracture topography determination using profilometry (Brown and Scholz, 1985a, b; Matsuki, 1999), X-ray computer tomography (Kling et al.,

55 2016), magnetic resonance imaging, and spectrophotometric analysis of epoxy replicas (Renshaw et al., 2000). All these methods can only be performed at the laboratory scale. Correlations between hydraulic and mechanical apertures were commonly established based on 3D information, providing a valuable understanding of the transport properties of fractures (Renshaw, 1995; Barton and de Quadros, 1997; Xiong et al., 2011; Kling et al., 2017). Nevertheless, outcrop studies can only provide single fracture profiles rather than an entire fracture configuration and the question addressed here is whether one can

60 reliably estimate hydraulic properties based on representative fracture profiles. Accordingly, hydraulic fracture apertures derived by the aforementioned methods have to be compared and evaluated regarding their reliability.

In this study, a systematic comparison of three different methods to determine hydraulic fracture apertures using 1) a flow-through apparatus, 2) a transient-airflow permeameter, and 3) a microscope camera was therefore performed on the same set of sandstone samples to evaluate the reliability, accuracy, and comparability of the results. Hydraulic aperture was measured

65   on various types of artificially induced single rock fractures, i.e., mismatched rough tensile fractures with defined relative

offsets, a matched rough tensile fracture, a saw-cut rough fracture, and a saw-cut smooth fracture. Hence, the purpose of this

study is a methodological comparison rather than a study on specific rock types.

2 Materials and methods

2.1 Rock samples

70   Five cylindrical sandstone core samples, namely Fontainebleau sandstone (e.g., Saadi et al., 2017) (labeled FOF1 and FOF4)

and Flechtinger sandstone (e.g., Fischer et al., 2012) (labeled FF2, FF3 and FF4) ~~with~~ 30 mm in diameter and 40 mm in length

were prepared for this study. The porosity and the average pore diameter, as determined by mercury intrusion porosimetry, of

the present Fontainebleau and Flechtinger sandstones are 2.3 % / 0.7 μm and 9.4 % / 3.8 μm, respectively. Both rocks are

characterized by a ~~very~~ low matrix permeability in the order of 10^{-18} m^2 as derived from previous measurements. Single tensile

75   fractures or saw-cut fractures were artificially induced along the sample axis (Fig.1). Tensile fractures in FOF1, FF2 and FF3

were induced using a Brazilian test setup yielding negligible edge damage at a displacement rate of 2×10^{-6} m/s. The separated

halves were subsequently assembled with or without installing PEEK gaskets on the top and bottom of the sample to create

fixed displacements with pre-offsets of 0.75 mm (FOF1) and 0.20 mm (FF2). The two halves of sample FF3 were matched

without offset. Samples FF4 and FOF4 contained a single saw-cut fracture. Due to the larger pore size and higher porosity of

80   Flechtinger sandstone, the fracture roughness of FF4 is significantly higher compared to that of FOF4. A heat-shrink tubing

was used to jacket the samples comprising a thin metal sheet placed between the fracture gap and the jacket to minimize a risk

of jacket rupture when the sample is under pressure in the flow-through apparatus. For all measurements, the samples were

constrained by this heat-shrink tubing ensuring the comparability between methods as the respective fracture configuration

was identical in each case.

Figure 1: **Strategy of sample preparation. The number of stars qualitatively indicates the relative intensity of surface roughness and fracture aperture. The upper and lower sample surfaces were used for the measurements of the mechanical aperture. a) FOF1, tensile fracture with a pre-offset of 0.75 mm along the sample axis; b) FF2, tensile fracture with a pre-offset of 0.2 mm; c) FF3, matched tensile fracture; d) FF4, saw-cut rough fracture; e) FOF4, saw-cut smooth fracture.**

2.2 Experimental methods

As shown in Fig. 2, three different experimental devices were used to investigate the hydraulic aperture of the five samples, namely 1) a flow-through apparatus (FTA; Fig. 1a), 2) a transient-airflow permeameter (TP; Fig. 1b), and 3) a microscope camera (MC; Fig. 1c). All samples were measured with each method in the order of FTA, TP, and MC. A brief outline of the three devices and the respective methods is provided subsequently.
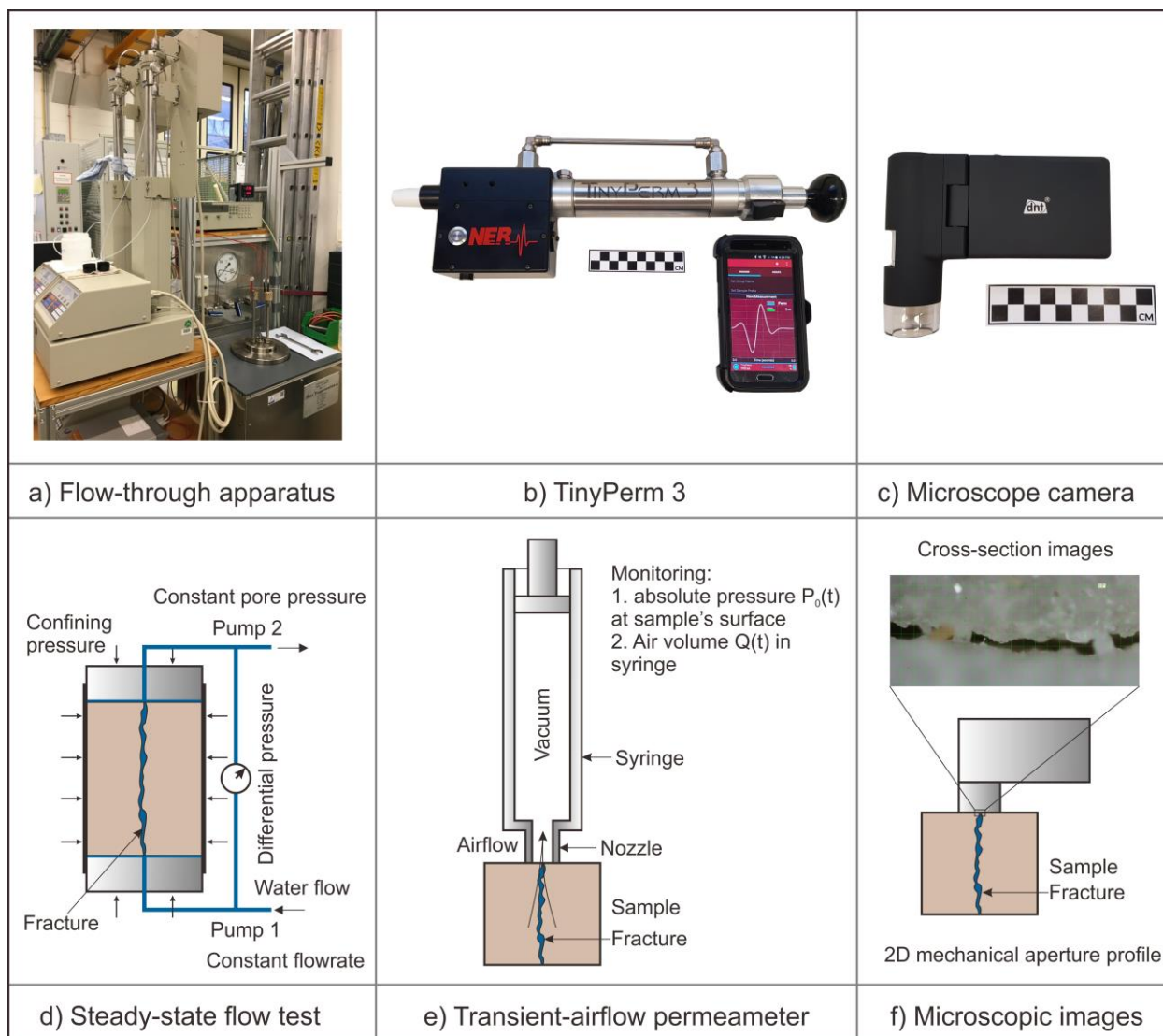
Figure 2: Images of experimental devices a) – c) and illustration of the applied methods used for the hydraulic fracture aperture measurements d) – f). a) Flow-through apparatus; b) portable transient-airflow permeameter ("TinyPerm 3"); c) microscope camera; d) steady-state flow test with a) to determine hydraulic aperture based on the "cubic law"; e) hydraulic aperture measured with b) by transient air withdrawal from the rock sample to the vacuum syringe; f) 2D mechanical aperture profile observed with c).

2.2.1 Flow-through apparatus

The absolute liquid (water) permeability of the fractured core samples was measured using a flow-through apparatus (FTA), as shown in Fig. 2a (Milsch et al., 2008), where the jacketed sample core is mounted in a pressure vessel (Fig. 2d). The hydrostatic confining pressure is generated with silicon oil using a syringe pump (ISCO 65D). The pore pressure is controlled by a downstream pump (ISCO 260D) set at constant pressure mode. The upstream pump (ISCO 260D) is connected to the

inlet at the lower end of the sample providing a constant fluid flow rate. During a flow-through experiment the pressure difference between the sample ends is monitored by a differential pressure transducer (IPD 40, ICS Schneider Messtechnik) with a measurable range of 0.0-0.6 MPa and an accuracy of < 0.2 %. Deionized water was used as the pore fluid and the permeability of the sample k_{sample} was evaluated using Darcy's Law (Darcy, 1856):

$$k_{sample} = \frac{Q\mu L}{\Delta p \cdot A} \tag{1}$$

where Q, μ, L, Δp are the flow rate, the dynamic fluid viscosity, the sample length, and the differential pressure between the sample ends, respectively. $A = \pi r^2$ is the cross-sectional area of the sample. In case the matrix permeability is very small compared to the fracture permeability, it is reasonable to assume that the total amount of flow through the sample is equal to the flow through the artificial fracture (Hofmann et al., 2016). Then:

$$k_{sample} \cdot (\pi r^2) = k_f \cdot (2r a_{FTA}) \tag{2}$$

where k_f is the fracture permeability and a_{FTA} is the hydraulic aperture as obtained by the flow-through experiment. Based on the "cubic law" and the assumption of laminar flow through the fracture, fracture permeability can be expressed as $k_f = a_{FTA}^2/12$ (Witherspoon et al., 1980). Hydraulic aperture can subsequently be derived by substituting k_f in Eq. (2) yielding:

$$a_{FTA} = \sqrt[3]{6\pi r k_{sample}} \tag{3}$$

2.2.2 Transient-airflow permeameter

A transient-airflow permeameter (TP; "TinyPerm 3" by New England Research Inc.) was used to independently determine the hydraulic fracture aperture of a sample (Fig. 2b). This portable device can be applied both in the laboratory and the field for direct measurements on core samples and outcrops, respectively. The theory of this device was derived by Brown and Smith (2013) yielding a response function H:

$$H = \frac{\int_{-\infty}^{\infty} Q(t) dt}{\int_{-\infty}^{\infty} P_0(t) dt} \tag{4}$$

where $Q(t)$ is the flow profile and $P_0(t)$ is the pressure profile, which both can be monitored by the device. Figure 2e shows the measurement principle. By pushing down the piston to create a vacuum within the chamber, air starts to flow from the sample to the syringe through the nozzle tip ultimately re-establishing atmospheric pressure conditions therein. Consequently, two time-dependent profiles $Q(t)$ and $P_0(t)$ can be obtained. It should be noted that the measured response function H is strongly related to the sample permeability and that other parameters, such as the geometry of the rock specimen, are also needed to ultimately determine permeability. Some of these parameters may be difficult to obtain, especially in the field. Thus, an empirical calibration of the device was conducted with an artificial fracture consisting of two polished granite samples whose aperture can be controlled by the thickness of feeler gauges in between, yielding (Brown and Smith, 2013):

$$T = -1.5 \log_{10}(a_{TP}) + 8.29 \tag{5}$$

where a_{TP} is the hydraulic fracture aperture, which is assumed equivalent to the known separation (i.e., the mechanical aperture) of the parallel granite plates, and T is a value obtained from a measurement with the TP, which is the common logarithm of

the final H when the pressure in the syringe returns to ambient pressure. Based on this empirical calibration and by directly measuring the response function H, hydraulic fracture apertures can be determined with this device (New England Research, 2015). The validity of this method was tested on parallel-plate fractures in the range between 20 μm and 2 mm, yielding a

140 insignificantly small uncertainty of ± 1.4% (Brown and Smith, 2013). Nevertheless, for natural rough fractures, to our knowledge, no validation and also no precision assessment have been performed yet.

2.2.3 Microscope camera

Mechanical aperture can be determined by measuring the vertical distances between the upper and lower fracture walls perpendicular to a predefined global reference plane (Hakami and Larsson, 1996) or by measuring the separation distances

145 oriented perpendicular to the local trend of the fracture walls (Mourzenko et al., 1995; Ge, 1997) as illustrated in Fig. 3. Konzuk and Kueper (2004) compared the two methods with the same fracture aperture revealing that the mean local perpendicular aperture is about 8% smaller than the mean global vertical aperture, while their aperture histograms essentially yield similar shape.

In this study, due to the fact that the microscopic images only represent small segments of the fracture in a sample, one cannot

150 unequivocally define a global reference plane that would fit all images. Therefore, an estimation of the local perpendicular distance between the adjacent fracture walls was used to maintain consistency in the analysis between individual images. 2D aperture profiles were manually obtained at the sample end faces (Fig. 2c, f) using a microscope camera (MC; DigiMicro Mobile, dnt GmbH). Applying the software "PortableCapture", the perpendicular distance a_i (Fig. 3) between the captured fracture edges was measured at 20 equidistant spots on the picture defined by a mesh grid. Knowing the magnification factor

155 of the microscope camera, the true distance between the fracture walls can be calculated for each spot. The magnification factors ranged between 200 and 206, corresponding to an investigated area of 1.72×2.29 mm^2 to 1.67×2.23 mm^2, respectively. More details can be found in (Hale et al., 2019). The mechanical fracture aperture a_m corresponds to the arithmetic mean of the measured distances in each image and was calculated by:

$$a_m = \frac{1}{n}\sum_{i=1}^{n} a_i \tag{6}$$

160
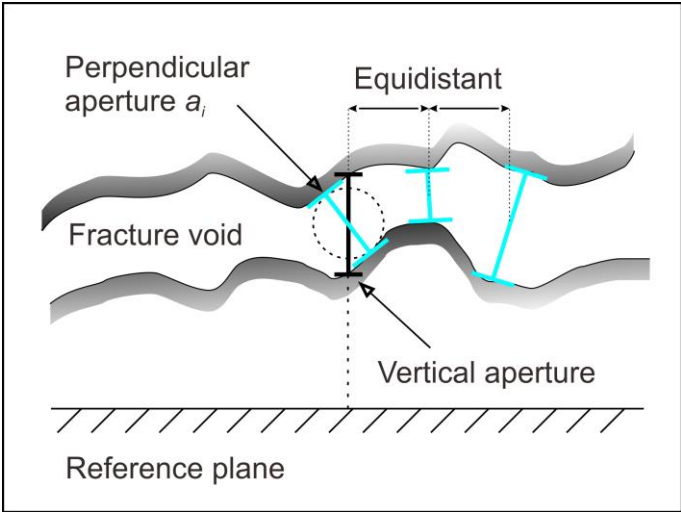
Figure 3: Conceptual illustration of different mechanical aperture definitions and the estimation method applied in this study (indicated in blue); modified from Konzuk and Kueper (2004).

Empirical equations based on a_m and the standard deviation of measured aperture values σ_a were subsequently used to estimate

165   the hydraulic aperture a_h (Table 1).

Table 1. Summary of empirical equations used to estimate hydraulic fracture apertures from measured mechanical apertures.

No.	Equation	Fracture type	Reference
1	$a_h = a_m \left(1 + \dfrac{\sigma_a^2}{a_m^2}\right)^{-\frac{1}{2}}$	Theoretical equation based on stochastics for lognormal aperture distribution	Renshaw (1995)
2	$a_h = \dfrac{a_m}{\sqrt[3]{1 + 20.5 \left(\dfrac{\sigma_a}{2a_m}\right)^{\frac{3}{2}}}}$	Natural granite fractures	Barton and de Quadros (1997)
3	$a_h = a_m \cdot \sqrt[3]{1 - \dfrac{1.13}{1 + 0.191 \left(\dfrac{2a_m}{\sigma_a}\right)^{1.93}}}$	Tensile granite fracture	Matsuki (1999)
4	$a_h = a_m \cdot \sqrt[3]{1 - \dfrac{\sigma_a}{a_m}}, \ \dfrac{\sigma_a}{a_m} < 1$	Replicas of a split sandstone and natural granite fracture	Xiong et al. (2011)
5	$a_h = a_m \cdot \left(1 + \dfrac{\sigma_a}{a_m}\right)^{-\frac{3}{2}}$	Numerical model of fracture sealing by hydrothermally grown quartz	Kling et al. (2017)

Note: a_h is estimated based on the relative roughness of a fracture, which can be expressed as the ratio between the standard deviation σ_a and the corresponding arithmetic mean mechanical aperture a_m.

170 Based on the analysis of all microscopic images for each sample, the mechanical aperture distribution can additionally be determined. As the minimum measurable distance was limited to 10 μm, one can apply a threshold of 10 μm, where mechanical apertures smaller than the threshold are considered as contacting asperities (Hakami and Larsson, 1996). Consequently, the contact area ratio R_c can be derived by quantifying the ratio of the number of contacting asperities and the total number of a_i. By assuming circular contact areas of the asperities oriented in parallel to the fracture plane, a hydraulic aperture a_H can be

175 obtained from the total mean mechanical aperture and R_c as follows (Walsh, 1981; Zimmerman et al., 1992):

$$a_H^3 = \frac{1-R_c}{1+R_c} a_m^3 \tag{7}$$

2.3 Experimental procedures

For the flow-through experiments the assembled rock samples were vacuum-saturated with deionized water in a desiccator. The specimen assembly was mounted in the pressure vessel of the FTA for the permeability measurements. The confining

180 pressure was first increased to 4 MPa and, subsequently, the pore pressure was increased to 1 MPa and maintained constant throughout the measurement. The confining pressure was then increased to 5 MPa, implying that the effective pressure applied to the sample was 4 MPa as the starting condition. It is well known that a first loading ramp causes the largest irreversible aperture closure as compared to further loading-unloading sequences (Hofmann et al., 2016; Milsch et al., 2016). In this study, one confining pressure loading-unloading cycle from 5 MPa to 30 MPa and back to 5 MPa (FOF1) or 2 MPa (FOF4, FF2,

185 FF3, and FF4) was performed at room temperature. The sample permeability was measured at each pressure step in defined confining pressure intervals. Due to the fact that the samples were subject to near-zero effective pressure when applying the other two methods (TP and MC), the hydraulic apertures at zero effective pressure were obtained from curve-fitting of the measured data during unloading (Sect. 3.1; Fig. 4) and used for comparison.

After completion of the flow-through experiment, the respective specimen assembly was removed from the pressure vessel.

190 The plugs and gaskets were taken off to expose the end faces of the samples for the subsequent TP measurements. The heat-shrink tubing, however, was kept in place in order to fasten the two halves of the specimen. The samples were then dried in an oven at 60 °C for several days to obtain defined test conditions for the TP measurements. The hydraulic fracture aperture a_{TP} was finally measured with the TP at ambient pressure and temperature conditions. Since the inner diameter of the TP's rubber nozzle is 8 mm and the diameter of the core was 30 mm, the effective cross-sectional area for the airflow is significantly

195 smaller than the total cross-sectional area of the core sample as investigated in the flow-through experiments. Thus, the hydraulic aperture was measured ten times on both the top and bottom end faces of the sample in order to fully cover the fracture across the sample diameter.

Finally, mechanical aperture profiles on both sample end faces were determined with the MC. 13 to 17 images were taken on each surface, namely 26 to 29 images in total for each sample, to fully cover the aperture profile across the sample diameter.

200   It should be recalled that all samples were tested by TP and MC after the flow-through experiments (FTA) yielding identical
fracture configurations and nearly identical measurement conditions for evaluating the hydraulic apertures determined by the
three methods.

3 Results and discussion

In the following two sub-sections the hydraulic aperture data as determined in this study is presented (Section 3.1) and

205   compared ~~with respect to the comparability of applied~~ measurement methods (Section 3.2). All data related to this publication
~~is~~ attached as Supplementary Material.

3.1 Measured hydraulic fracture apertures

The FTA experiments and the TP measurements represent direct methods for determining hydraulic fracture aperture. Figure
4 shows the hydraulic apertures measured with the FTA (a_{FTA}) at different effective pressures during unloading. Subsequently,

210   the hydraulic apertures at zero effective pressure were predicted by extrapolation of the different unloading sequences, yielding
65.9 µm for FOF1, 37.0 µm for FF2, 9.8 µm for FF3, 47.6 µm for FF4, and 7.7 µm for FOF4, respectively. The mismatched
rough fractures (FOF1 and FF2) and the saw-cut rough fracture (FF4) are characterized by relatively large hydraulic apertures,
whereas the matched rough fracture (FF3) and the saw-cut smooth fracture (FOF4) yield significantly smaller and nearly
identical hydraulic apertures.
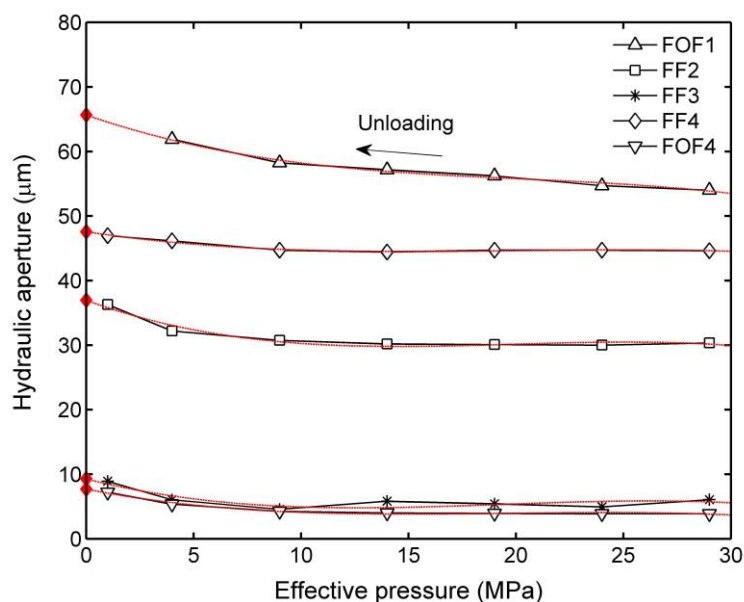
215

Figure 4: Hydraulic aperture a_{FTA} as a function of effective pressure during unloading. Each point is a steady-state permeability measurement at the respective effective pressure. The fitted curves (red lines) yield the sample dependent hydraulic aperture at zero effective pressure (red diamonds).

Figure 5 shows the hydraulic apertures a_{TP} determined with the TP, where the results show higher variability for the samples

220 with larger apertures (FOF1, FF2, and FF4) in contrast to the samples with smaller apertures (FF3 and FOF4). Since the nozzle of the TP is smaller in size than the cross-sectional area of the present core samples, the individually measured hydraulic aperture values do not necessarily represent the hydraulic aperture of the entire sample. However, the range of the hydraulic aperture values of each sample can serve as an indicator for the variability of hydraulic aperture along the fracture width. Samples FF3 and FOF4 only show insignificant variations resulting from the matched and smooth surfaces, respectively,

225 indicating a rather constant aperture across the samples.
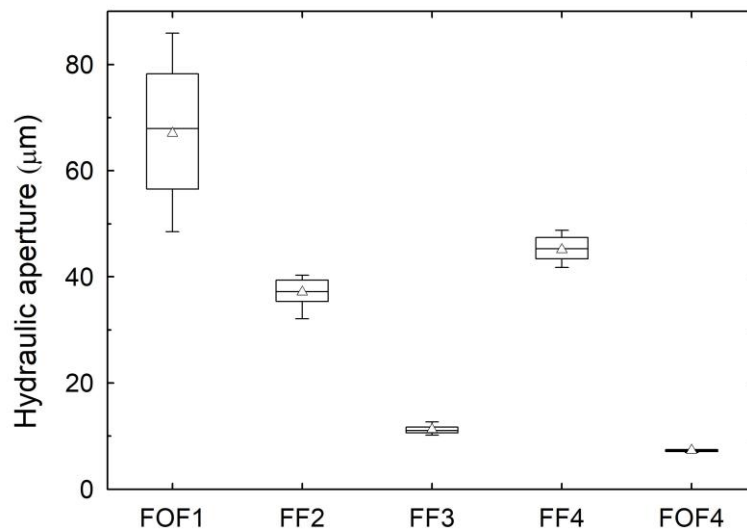
Figure 5: Hydraulic aperture of each sample measured with the transient-airflow permeameter (TP), including a total of 20 values for each sample taken at the top and bottom end faces (Fig. 1). The solid line and the open triangle in the box indicate the median and mean of each dataset, respectively.

230 Figure 6 shows representative microscopic images of the fractures taken with the MC. The 2D mechanical aperture a_m in each image was measured by determining the distance between the upper and lower fracture wall at 20 evenly spaced spots. The arithmetic mean of the measured distances in each image was subsequently calculated representing the mean mechanical fracture aperture of the observed area. The mechanical apertures derived from all profile images of each sample are shown in Fig. 7, yielding significantly larger variations in aperture values in comparison to the corresponding TP hydraulic apertures

235 a_{TP} (Fig. 5).
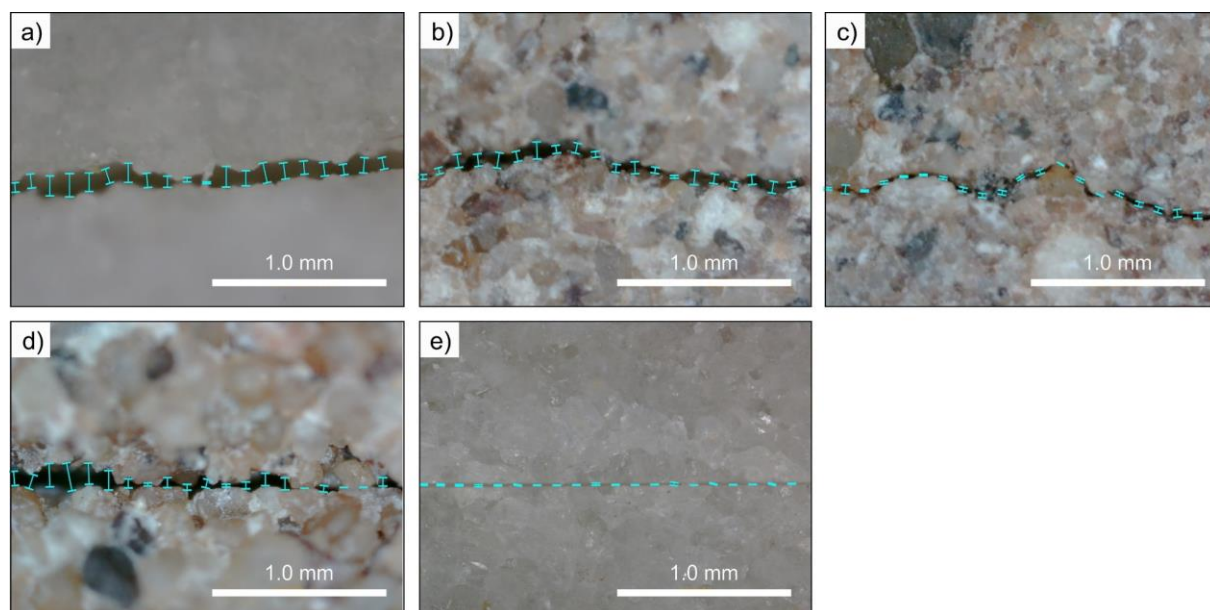
Figure 6: Representative microscopic images of the samples comprising parts of the respective fracture. a) FOF1, with a pre-offset of 0.75 mm; b) FF2, with a pre-offset of 0.2 mm; c) FF3, matched rough fracture; d) FF4, saw-cut rough fracture; e) FOF4, saw-cut smooth fracture. The distances between the upper and lower fracture walls were measured at equidistant locations.

240
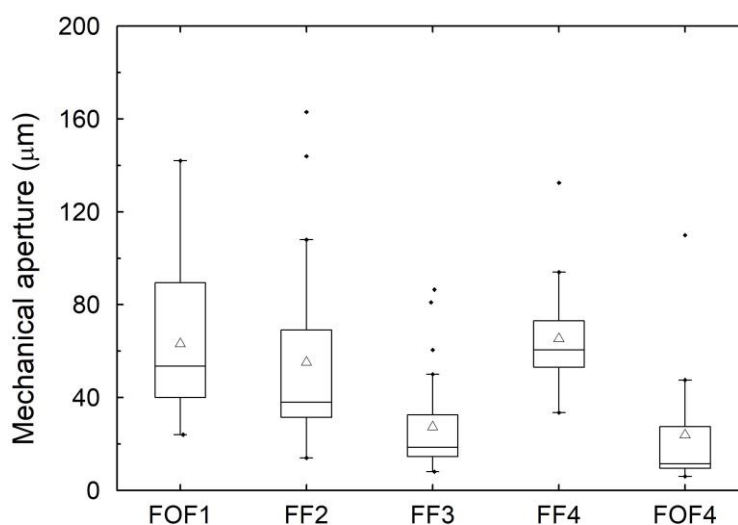
Figure 7: Mechanical apertures of the samples derived from image series taken on the top and bottom end faces with the microscope camera (MC). The solid line and the open triangle in the box indicate the median and mean of each dataset, respectively.

From the totality of measured distances based on all 2D microscope images of each sample, their respective mechanical aperture distributions can be derived as shown in Fig. 8. The contact area ratio R_c of samples FOF1, FF2, FF3, FF4, and FOF4

245 is 0.142, 0.173, 0.186, 0.054, and 0.150, respectively, as resulting from the loading-unloading cycle in the FTA. As expected, the matched fracture surfaces of FF3 exhibit the largest contact area ratio compared to all other samples. The hydraulic aperture

a_H can be subsequently derived with Eq. (7) using the corresponding total mean mechanical aperture as well as R_c. The resulting hydraulic apertures of FOF1, FF2, FF3, FF4, and FOF4 are 57.4 µm, 49.1 µm, 24.1 µm, 63.0 µm, and 21.5 µm, respectively. Based on the former total mean mechanical apertures and their standard deviations, hydraulic apertures were

250   additionally evaluated using the empirical equations listed in Table 1 as outlined and discussed in Sect. 3.2 below.
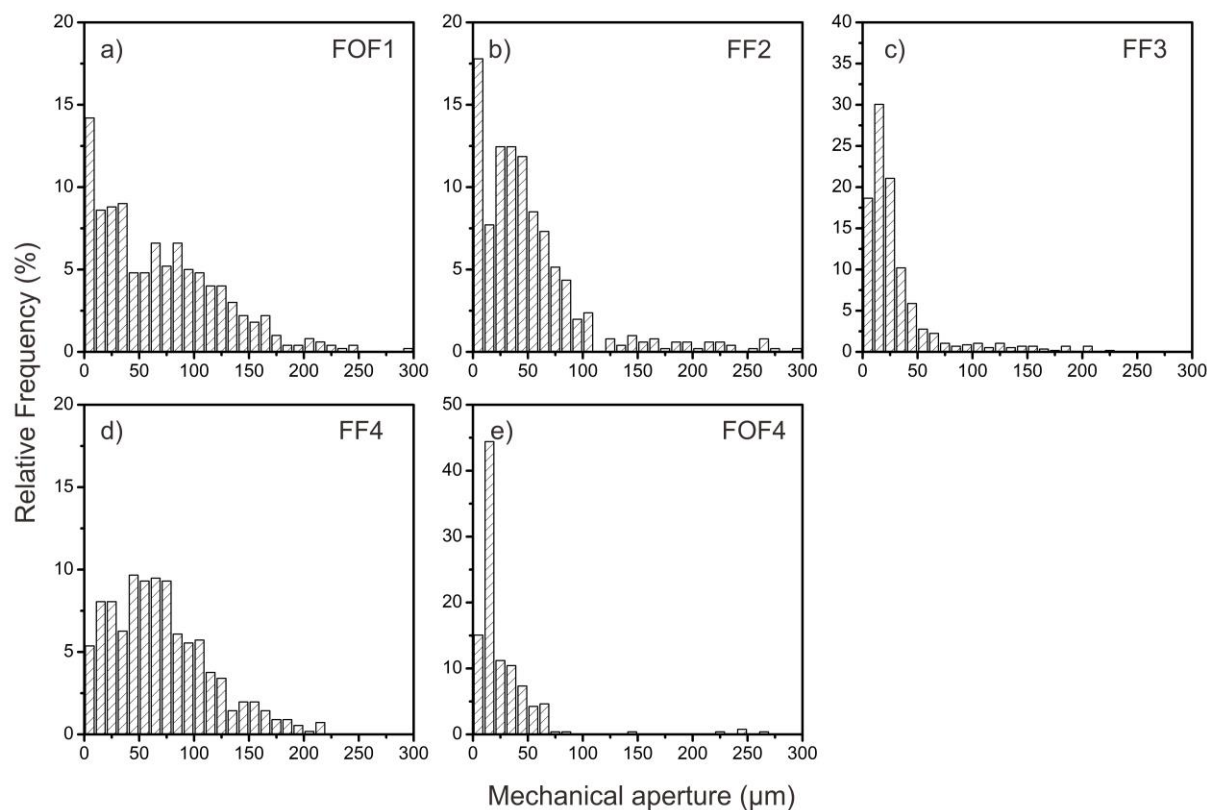
Figure 8: Frequency histograms showing the mechanical aperture distribution obtained from the 2D microscopic images of each sample. a) FOF1; b) FF2; c) FF3; d) FF4; e) FOF4.

3.2 Comparison of hydraulic fracture apertures

255   Figure 9 presents an overall comparison of hydraulic apertures of all samples measured with the FTA, the TP, and the MC. The mean and median hydraulic apertures a_{TP} determined with the transient-airflow permeameter are consistent with the absolute hydraulic apertures a_{FTA} determined by flow-through experiments. Furthermore, it can also be seen that the smaller the hydraulic aperture, the smaller the range of variations. For all samples, the hydraulic apertures a_h derived from the empirical equations listed in Table 1 using the ~~individual~~ mean mechanical aperture and the corresponding standard deviation from each

260   microscopic image ~~show~~ larger variations in comparison to the hydraulic apertures measured with both the FTA and the TP. This is likely due to the fact that for each individual microscopic image only a 2.29 mm wide part of the fracture was considered, which does not represent the studied fracture over its entire width.
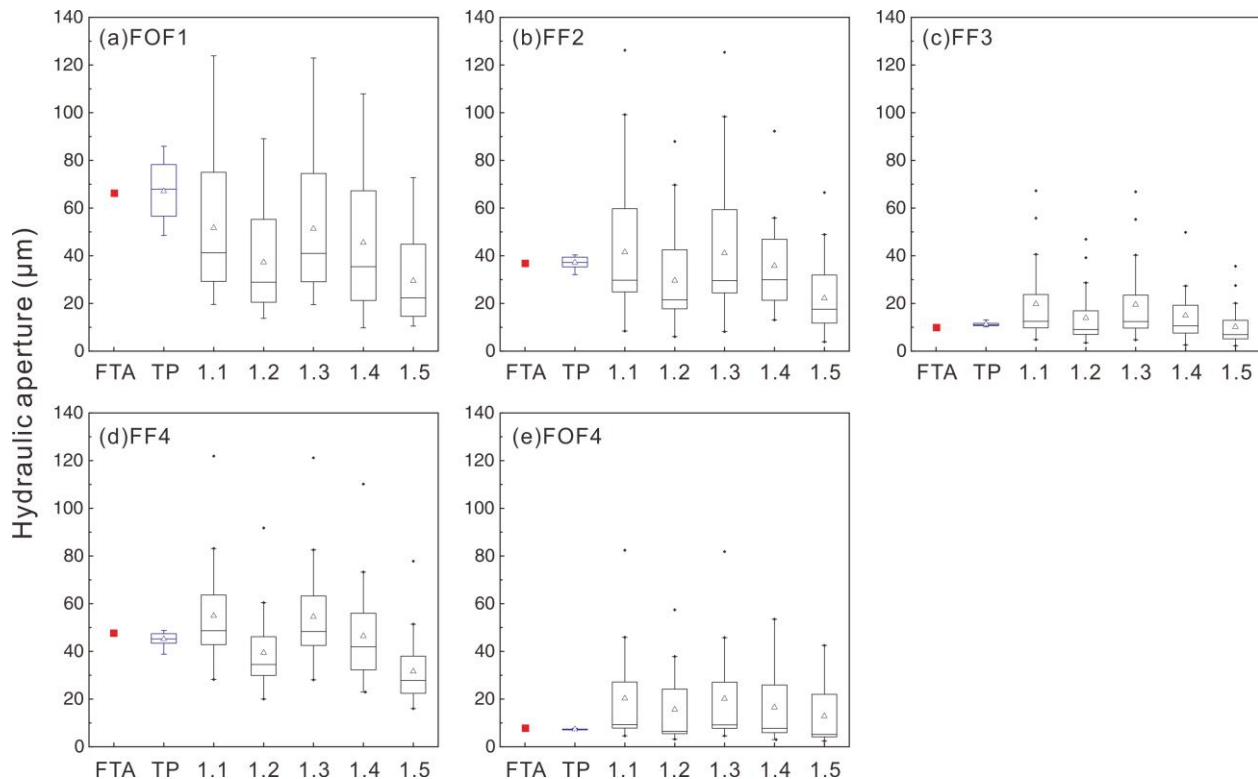
Figure 9: Comparison of hydraulic apertures measured with the flow-through apparatus (FTA; red squares), the transient-airflow permeameter (TP; blue box plot), and derived from MC-measured mechanical apertures (1.1 to 1.5; black box plots) using the empirical equations 1 to 5 listed in Table 1 for samples: a) FOF1; b) FF2; c) FF3; d) FF4; e) FOF4.

Figure 10 shows the correlation between the hydraulic apertures a_{TP} measured with the TP and a_{FTA} obtained by the FTA. For each sample, the mean and median values of the TP measurements are in excellent agreement with the ones measured with the FTA. It is noted that all measured a_{TP} of sample FF3 are slightly larger than the determined a_{FTA}. Due to the well-matched rough fracture surfaces of FF3, the fracture aperture is significantly smaller in comparison to the other samples (except FOF4). Hence, already a small applied stress may result in a comparatively significant aperture decrease and the predicted zero-stress aperture a_{FTA} of FF3 might therefore be slightly underestimated. However, this small discrepancy should be acceptable when the TP is applied in the field. Based on this comparison one can infer that measurements with both the FTA and the TP would yield an even better agreement when hydraulic apertures are determined at elevated stress conditions as a result of an enhanced stability of the respective fracture configuration. In addition, the standard deviations σ_a of the hydraulic apertures a_{TP} of samples FOF1, FF2, FF3, FF4, and FOF4 are 12.0 μm, 2.3 μm, 0.9 μm, 2.6 μm, and 0.3 μm, respectively, which clearly demonstrates that for smaller hydraulic apertures less variability of measured values can be observed.

As mentioned before, for TP measurements of hydraulic aperture (a_{TP}), the effective sampled area of the rubber nozzle in contact with the sample surface is smaller than the sample's cross-sectional area. Consequently, the results, particularly for samples with a larger hydraulic aperture, show substantial variations. However, by conducting multiple measurements to fully

cover the entire cross-sectional area, the mean and median hydraulic aperture a_{TP} and the corresponding absolute hydraulic aperture a_{FTA} showed an excellent agreement. The investigation depth of the transient-airflow permeameter for isotropic porous media was estimated to be approximately twice the internal radius of the nozzle tip (Goggin et al., 1988; Jensen et al., 1994; Possemiers et al., 2012) since the largest pressure gradient along a sample occurs near the injection/extraction region. This implies that a certain minimum sample length (i.e., twice the internal radius of the nozzle tip) is required for a reliable permeability measurement. However, for fractures, this minimum length has not been established yet. As mentioned before, the calibration of the TP was performed by using parallel plates as idealized fractures. Increasing the fracture length has no effect on this idealized aperture while a minimum length of the fracture might be required for sufficient airflow. As the length of the measured core samples was 40 mm (i.e., ten times the nozzle tip radius), the total fracture volume was only partially covered during a TP measurement provided that the investigation depth in single fractures is comparable to the one in porous media. Overall, the accuracy and the reliability of hydraulic aperture results obtained from TP measurements can be significantly improved by performing repeated measurements along the fracture width as well as a subsequent statistical evaluation. Nevertheless, a rough fracture in a core longer than 40 mm may lead to less conformity of a_{FTA} and a_{TP} since the transient airflow does not fully cover the entire fracture area.
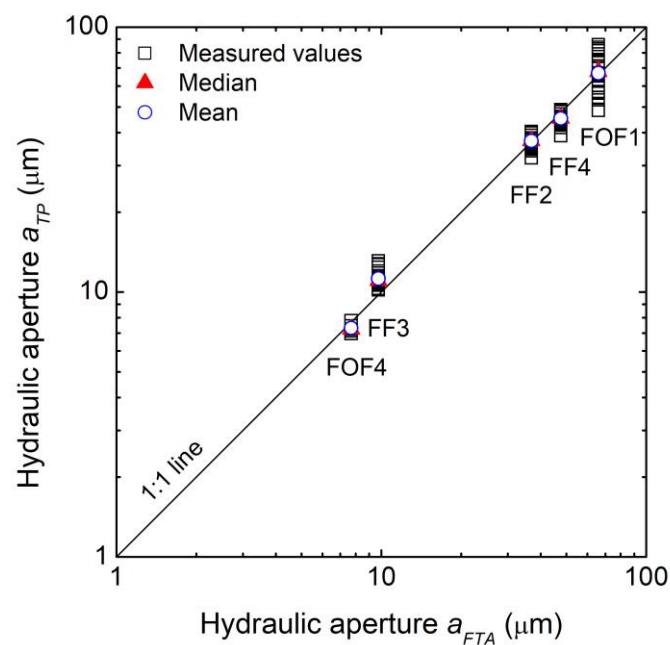
Figure 10: Cross-plot of the hydraulic apertures a_{TP} determined with the transient-airflow permeameter (TP) and the hydraulic apertures a_{FTA} measured with the flow-through apparatus (FTA).

Figure 11 shows the correlations between the hydraulic aperture a_{FTA} (FTA) and the median (a) and mean (b) hydraulic apertures a_h derived from measured mechanical apertures (MC) when applying the empirical equations listed in Table 1. For

300   the relatively narrow fractures in FOF4 and FF3 with hydraulic apertures around 10 μm, the median of a_h does replicate the actual hydraulic aperture obtained from the flow-through experiments very well, especially when using the equations of Barton and de Quadros (1997) and Xiong et al. (2011). In contrast, the mean of a_h overestimates the respective FTA hydraulic aperture. For the relatively open fractures in FOF1, FF2, and FF4 with hydraulic apertures larger than 30 μm, the arithmetic mean is in better agreement with the respective FTA hydraulic aperture. Overall, it can be concluded that the equations of Barton and de

305   Quadros (1997) and Xiong et al. (2011) yield better matching results for the studied samples as compared to the other equations listed in Table 1.

When additionally deriving the contact area ratio from all images of each sample, Eq. (7) can be applied and compared to the results of hydraulic apertures as calculated using the empirical equations in Table 1 (Fig. 11 c). For samples with hydraulic apertures smaller than 10 μm, the derived results overestimate the actual aperture (a_{FTA}) except for Kling et al. (2017). For

310   hydraulic apertures larger than 30 μm, the derived results almost exclusively underestimate the true values with the exception of those obtained from Eq. (7). Possible errors regarding the input data may be related to the size limit of each microscopic image, where the obtained data can only represent the fracture aperture within the individually observed area with a segment width of 2.29 mm. Also, since the mechanical aperture distribution and the contact area ratio are obtained from 2D images of the fracture profiles, these do not fully represent the true fracture aperture distribution and contact area ratio in 3D.

315   Nevertheless, the hydraulic apertures of the different samples as derived from the same respective equation are comparable and reflect the relative aperture differences.
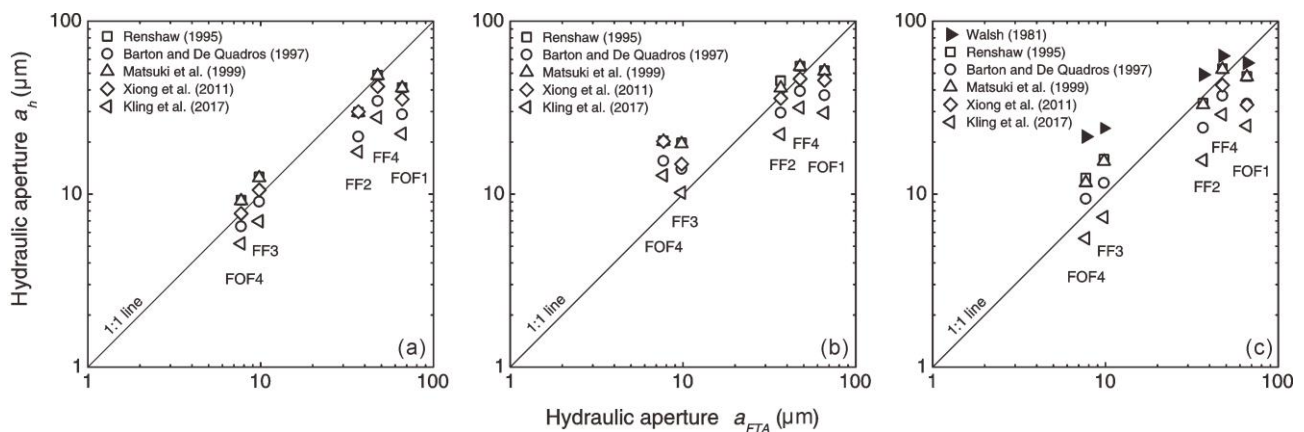
Figure 11: Cross-plots of calculated hydraulic apertures and hydraulic apertures a_{FTA} measured with the flow-through apparatus
320   **(FTA). a) Median and b) mean hydraulic apertures a_h using MC-based mechanical apertures of each image in combination with the equations listed in Table 1. c) As in a), but hydraulic apertures a_H derived from Eq. (7) (black triangles) are additionally shown for comparison.**

4 Conclusions

325   Three different methodological approaches for hydraulic fracture aperture determination, i.e., using a flow-through apparatus
(FTA), a transient-airflow permeameter (TP), and a digital microscope camera (MC), were applied and compared. A total of
five (Fontainebleau and Flechtinger) sandstone samples containing single fractures of different types and representing a
hydraulic aperture range between 8 µm and 66 µm were investigated. The comparison of the results aimed at assessing the
applicability, reliability, and accuracy of each method yielding the following conclusions:

330   1. The agreement of the mean hydraulic apertures determined with the transient-airflow permeameter (a_{TP}) and the
corresponding hydraulic apertures measured by flow-through experiments (a_{FTA}) was excellent for all samples.

2. For rough fractures with hydraulic apertures larger than 30 µm, measurements with the transient-airflow permeameter
have to be repeated across the full fracture width in order to statistically obtain reliable results. The investigations
additionally showed that this permeameter can also be reliably used to determine hydraulic fracture apertures as small
335   as approximately 5 µm.

3. The hydraulic apertures estimated by evaluating 2D mechanical aperture profiles in digital microscope camera images
showed large variations for all samples and therefore cannot be directly compared to the results obtained by the two
other approaches. On the other hand, when applying empirical equations taken from literature, the derived mean and
median hydraulic apertures are intercomparable for the respective correlation and correctly reflect the relative aperture
340   differences between the fracture types.

In summary, hydraulic fracture apertures can be measured directly and precisely, also as a function of pressure and temperature,
by performing flow-through experiments in appropriate apparatuses. For a large number of routine measurements at ambient
conditions this procedure, however, is time-consuming and costly. For such purposes, this study shows that the transient-
airflow permeameter offers a fast and highly efficient approach for accurate hydraulic aperture determination. For the first
345   time this study quantitatively evaluated the reliability and precision of transient-airflow permeameter measurements on natural
rough fractures extending previous calibrations based on ideal parallel plates (Brown and Smith, 2013). When following an
optical approach using a digital microscope camera, qualitatively correct estimates of hydraulic aperture variations both along
a fracture and between different fracture types are obtained. Although conclusions here are drawn from laboratory scale
measurements on core samples, these should also be valid when applying the mobile methods (TP and MC) on fractures
350   displaying the same aperture range at the outcrop scale. Hence, integrating the results of hydraulic aperture measurements on
fractures, both, from core samples and outcrops applying multiple methods will improve our understanding of permeability in
fractured rock.

355 CC prepared all rock samples and performed the experiments with the FTA. SH conducted the TP and MC measurements on the same specimens. All authors (CC, SH, HM, and PB) analyzed and interpreted the results and contributed to drafting the manuscript.

Competing interests

The authors have no competing interests to declare.

360 **Data availability**

All data related to this manuscript is attached as Supplementary Material.

Acknowledgments

The authors thank Christian Kluge and Michael Naumann (GFZ Potsdam) for technical support during sample preparation. Chaojie Cheng acknowledges funding by the China Scholarship Council (CSC) under grant No. 201606410056. Financial

365 support by the German Federal Ministry of Education and Research (BMBF) under grant No. 03G0871D, as part of the ResKin (Reaction Kinetics in Reservoir Rocks) project, is also gratefully acknowledged.

References

Barton, N. and de Quadros, E. F.: Joint aperture and roughness in the prediction of flow and groutability of rock masses, Int. J. Rock Mech. Min. Sci., 34, 252. e251-252. e214, doi: 10.1016/S1365-1609(97)00081-6, 1997.

370 Brown, S. and Smith, M.: A transient-flow syringe air permeameter, Geophysics, 78, D307-D313, doi: 10.1190/Geo2012-0534.1, 2013.

Brown, S. R. and Scholz, C. H.: Broad bandwidth study of the topography of natural rock surfaces, J. Geophys. Res.-Sol. Ea., 90, 12575-12582, doi: 10.1029/JB090iB14p12575, 1985a.

Brown, S. R. and Scholz, C. H.: Closure of random elastic surfaces in contact, J. Geophys. Res.-Sol. Ea., 90, 5531-5545, doi:

375 10.1029/JB090iB07p05531, 1985b.

Darcy, H.: Les fontaines publique de la ville de Dijon, Dalmont, 1856.

Fischer, C., Dunkl, I., von Eynatten, H., Wijbrans, J. R., and Gaupp, R.: Products and timing of diagenetic processes in Upper Rotliegend sandstones from Bebertal (North German Basin, Parchim Formation, Flechtingen High, Germany), Geol. Mag., 149, 827-840, doi: 10.1017/S0016756811001087, 2012.

380   Ge, S.: A governing equation for fluid flow in rough fractures, Water Resour. Res., 33, 53-61, doi: 10.1029/96WR02588, 1997.

Goggin, D., Chandler, M., Kocurek, G. t., and Lake, L.: Patterns of permeability in eolian deposits: Page Sandstone (Jurassic), northeastern Arizona, SPE Format. Evalu., 3, 297-306, doi: 10.2118/14893-PA, 1988.

Hakami, E. and Larsson, E.: Aperture measurements and flow experiments on a single natural fracture, Int. J. Rock Mech. Min. Sci., 33, 395-404, doi: 10.1016/0148-9062(95)00070-4, 1996.

385   Hale, S., Naab, C., Butscher, C., and Blum, P.: Method comparison to determine hydraulic apertures of natural fractures, Rock Mech. Rock Eng., doi: 10.1007/s00603-019-01966-7, 2019.

Hofmann, H., Blocher, G., Milsch, H., Babadagli, T., and Zimmermann, G.: Transmissivity of aligned and displaced tensile fractures in granitic rocks during cyclic loading, Int. J. Rock Mech. Min. Sci., 87, 69-84, doi: 10.1016/j.ijrmms.2016.05.011, 2016.

390   Huysmans, M., Peeters, L., Moermans, G., and Dassargues, A.: Relating small-scale sedimentary structures and permeability in a cross-bedded aquifer, J. Hydrol., 361, 41-51, doi: 10.1016/j.jhydrol.2008.07.047, 2008.

Jensen, J., Glasbey, C., and Corbett, P.: On the interaction of geology, measurement, and statistical analysis of small-scale permeability measurements, Terra Nova, 6, 397-403, doi: 10.1111/j.1365-3121.1994.tb00513.x, 1994.

Kling, T., Huo, D., Schwarz, J.-O., Enzmann, F., Benson, S., and Blum, P.: Simulating stress-dependent fluid flow in a
395   fractured core sample using real-time X-ray CT data, Solid Earth, 7, doi: 10.5445/IR/1000059909, 2016.

Kling, T., Schwarz, J.-O., Wendler, F., Enzmann, F., and Blum, P.: Fracture flow due to hydrothermally induced quartz growth, Adv. Water Resour., 107, 93-107, doi: 10.1016/j.advwatres.2017.06.011, 2017.

Konzuk, J. S. and Kueper, B. H.: Evaluation of cubic law based models describing single-phase flow through a rough-walled fracture, Water Resour. Res., 40, doi: 10.1029/2003WR002356, 2004.

400   Matsuki, K.: Size effect in flow conductance of a small-scale hydraulic fracture in granite, Geoth. Sci. Tech., 6, 113-138, 1999.

Milsch, H., Spangenberg, E., Kulenkampff, J., and Meyhöfer, S.: A new apparatus for long-term petrophysical investigations on geothermal reservoir rocks at simulated in-situ conditions, Transport Porous Med., 74, 73-85, doi: 10.1007/s11242-007-9186-4, 2008.

Milsch, H., Hofmann, H., and Blocher, G.: An experimental and numerical evaluation of continuous fracture permeability
405   measurements during effective pressure cycles, Int. J. Rock Mech. Min. Sci., 89, 109-115, doi: 10.1016/j.ijrmms.2016.09.002, 2016.

Mourzenko, V. V., Thovert, J.-F., and Adler, P. M.: Permeability of a single fracture; validity of the Reynolds equation, J. de Phys. II, 5, 465-482, doi: 10.1051/jp2:1995133, 1995.

Neuzil, C. E. and Tracy, J. V.: Flow through fractures, Water Resour. Res., 17, 191-199, doi: 10.1029/WR017i001p00191,
410   1981.

New England Research, TinyPerm 3: available at: https://www.ner.com/site/systems/tinyperm3.html, 2015.

Possemiers, M., Huysmans, M., Peeters, L., Batelaan, O., and Dassargues, A.: Relationship between sedimentary features and permeability at different scales in the Brussels Sands, Geol. Belg., 15, 156-164, 2012.

Renshaw, C. E.: On the relationship between mechanical and hydraulic apertures in rough-walled fractures, J. Geophys. Res.-Sol. Ea., 100, 24629-24636, doi: 10.1029/95JB02159, 1995.

Renshaw, C. E., Dadakis, J. S., and Brown, S. R.: Measuring fracture apertures: A comparison of methods, Geophys. Res. Lett., 27, 289-292, doi: 10.1029/1999GL008384, 2000.

Rogiers, B., Beerten, K., Smeekens, T., Mallants, D., Gedeon, M., Huysmans, M., Batelaan, O., and Dassargues, A.: Derivation of flow and transport parameters from outcropping sediments of the Neogene aquifer, Belgium, Geol. Belg., 16, 129-147, 2013.

Rogiers, B., Beerten, K., Smeekens, T., Mallants, D., Gedeon, M., Huysmans, M., Batelaan, O., and Dassargues, A.: The usefulness of outcrop analogue air permeameter measurements for analyzing aquifer heterogeneity: quantifying outcrop hydraulic conductivity and its spatial variability, Hydrol. Process., 28, 5176-5188, doi: 10.1002/hyp.10007, 2014.

Saadi, F. A., Wolf, K.-H., and Kruijsdijk, C. v.: Characterization of Fontainebleau sandstone: quartz overgrowth and its impact on pore-throat framework, J Petrol. Envir. Biot., 08, doi: 10.4172/2157-7463.1000328, 2017.

Snow, D. T.: Anisotropie permeability of fractured media, Water Resour. Res., 5, 1273-1289, doi: 10.1029/WR005i006p01273, 1969.

Snow, D. T.: The frequency and apertures of fractures in rock, Int. J. Rock Mech. Min. Sci., 7, 23-40, doi: 10.1016/0148-9062(70)90025-2, 1970.

Walsh, J.: Effect of pore pressure and confining pressure on fracture permeability, Int. J. Rock Mech. Min. Sci., 18, 429-435, doi: 10.1016/0148-9062(81)90006-1, 1981.

Watkins, H., Bond, C. E., Healy, D., and Butler, R. W.: Appraisal of fracture sampling methods and a new workflow to characterise heterogeneous fracture networks at outcrop, J. Struct. Geol., 72, 67-82, doi: 10.1016/j.jsg.2015.02.001, 2015.

Witherspoon, P. A., Wang, J. S., Iwai, K., and Gale, J. E.: Validity of cubic law for fluid flow in a deformable rock fracture, Water Resour. Res., 16, 1016-1024, doi: 10.1029/WR016i006p01016, 1980.

Xiong, X., Li, B., Jiang, Y., Koyama, T., and Zhang, C.: Experimental and numerical study of the geometrical and hydraulic characteristics of a single rock fracture during shear, Int. J. Rock Mech. Min. Sci., 48, 1292-1302, doi: 10.1016/j.ijrmms.2011.09.009, 2011.

Zeeb, C., Gomez-Rivas, E., Bons, P. D., and Blum, P.: Evaluation of sampling methods for fracture network characterization using outcrops, AAPG bull., 97, 1545-1566, doi: 10.1306/02131312042, 2013.

Zimmerman, R. W., Kumar, S., and Bodvarsson, G. S.: Lubrication theory analysis of the permeability of rough-walled fractures, Int. J. Rock Mech. Min. Sci., 28, 325-331, doi: 10.1016/0148-9062(91)90597-F, 1991.

Zimmerman, R. W., Chen, D.-W., and Cook, N. G.: The effect of contact area on the permeability of fractures, J. Hydrol., 139, 79-96, doi: 10.1016/0022-1694(92)90196-3, 1992.